ISLAMIC UNIVERSITY OF TECHNOLOGY
ORGANIZATION OF ISLAMIC COOPERATION (OIC)

Macro-cell and Micro-cell Corrosion of Steel in Concrete with Different Interfacial Transition Zones (ITZ) and Variations of Seawater Concentrations

Name and ID

Maliha Mahjabin, 190051212

Md. Zawad Rafid, 190051227

Labiba Amin Parisa, 190051235

Mozidun Nahar Lorin, 190051241

A THESIS SUBMITTED FOR THE DEGREE OF BACHELOR OF SCIENCE IN CIVIL ENGINEERING (STRUCTURE)

DEPARTMENT OF CIVIL AND ENVIRONMENTAL ENGINEERING
ISLAMIC UNIVERSITY OF TECHNOLOGY (IUT)
2024

PROJECT APPROVAL

This is to certify that the thesis entitled “Macro-cell and Micro-cell Corrosion of Steel in Concrete with Different Interfacial Transition Zones (ITZ) and Variations of Seawater Concentrations” submitted by Maliha Mahjabin, Md. Zawad Rafid, Labiba Amin Parisa and Mozidun Nahar Lorin have been approved as partial fulfillment of the requirement for the Degree Bachelor of Science in Civil Engineering at the Islamic University of Technology (IUT).

Supervisor

Dr. Md. Tarek Uddin, P.Eng.
Professor
Department of Civil and Environmental Engineering (CEE)
Islamic University of Technology (IUT)
Board Bazar, Gazipur-1704, Bangladesh.

DECLARATION

We declare that the undergraduate research work described in this thesis was completed by us under the expert supervision of Professor Dr. Md. Tarek Uddin. We followed proper procedures to make sure the work is original and hasn't been copied from anywhere else. We've conducted our own research to ensure the originality of the information presented here.

MALIHA MAHJABIN
Student ID: 190051212

MD. ZAWAD RAFID
Student ID: 190051227

LABIBA AMIN PARISA
Student ID: 190051235

MOZIDUN NAHAR LORIN
Student ID: 190051241

DEDICATION

We dedicate this thesis to our parents whose significant time, endless support and sacrifices have been the cornerstone of our academic journey. They have inspired us to pursue our technological ambitions without ever looking back. We are eternally grateful to them.

We also like to express our gratitude to our esteemed supervisor, Professor Dr. Md. Tarek Uddin, for his unwavering support and motivation. This project could not have been accomplished without him.

ACKNOWLEDGEMENT

"In the name of Allah, Most Gracious, Most Merciful"

We are thankful to Almighty Allah for providing us with the opportunity to finish this thesis and for making it possible for us to find solutions to problems that arose during the course of our project work.

Our profound gratitude is extended to our supervisor, Dr. Md. Tarek Uddin, P.Eng., Professor, Islamic University of Technology, Department of Civil and Environmental Engineering for his gracious guidance, practical counsel and on-going assistance. His innovative and technical leadership was crucial to this research project's accomplishment. Without his guidance, the paper would never have been completed.

Furthermore, we want to express our sincere gratitude to all of the faculty members who have offered insightful advice during this thesis project. We would like to thank the lab instructors for all of their help and encouragement.

Table of Contents

List of Figures

List of Tables

List of Equations

$$I = \frac{V}{R} \tag{1}$$

$$I_{mac} = \frac{I}{A} \times 10^{6} \tag{2}$$

$$I_{mic} = \frac{B}{R_P} \times 10^{6} \tag{3}$$

$$B = \frac{\beta_a \beta_c}{2.3(\beta_a + \beta_c)} \tag{4}$$

$$D = 0.0116 \times I_{mac} \times t \tag{5}$$

$$I_{avg} = I_{mac(avg)} + I_{mic(avg)} \tag{6}$$

ABSTRACT

A comprehensive research examination was conducted to evaluate the chloride entrance in concrete by measuring the macro-cell and micro-cell corrosion of steel bars with varying interfacial transition zones and seawater concentrations. The interfacial transition zones were made by applying cement coating around the steel bars having different water-cement ratios and distinctive chloride concentrations. The study included ten scenarios and utilized cylindrical and prism examples, including a controlled case with uncoated steel rebar. The prism specimens comprised of three segmented steel bars and one continuous bar that were electrically connected to the outside of the specimens. This arrangement encouraged the steady observing of macro-cell corrosion current for 60 days utilizing a data logger. Taking after the measurement of macro-cell corrosion, the samples went through Limited wetting in a highly humid environment (99%), even with temperature variations (20°C to 40°C), resulted in minimal steel corrosion. However, submersion in seawater at 40°C caused rapid microcell corrosion, emphasizing the crucial role of electrolytes in accelerating the process. During these cycles, various parameters were measured, including half-cell potential along the steel bar, concrete resistance, macro-cell and micro-cell corrosion, and chloride concentration. A portable corro-map device was used to examine the micro-cell corrosion of the steel bars at 10-day intervals. After all examinations, the specimens were carefully cracked, and the steel bars were collected to assess the corroded area. Also, deposits were analyzed utilizing a Scanning Electron Microscope (SEM) and Energy Dispersive X-ray (EDX). Regardless of the specific case studied, macro-cell corrosion exhibited a consistent trend of decrease. Conversely, micro-cell corrosion displayed a tendency to increase with time. Coating steel bars initially showed promise in reducing corrosion, acting as a barrier against chloride ions. However, increased seawater content within the coating led to higher corrosion. This suggests coating degradation, possibly from chloride damage or pathways created by imperfections. The outcomes have implications for the durability of reinforced concrete. SEM revealed more voids and EDX confirmed rust at the steel-coating interface with higher water-cement ratio, however deposition of potentially ettringite, calcium hydride, and calcium monohydrate may reduce macro-cell corrosion.

Keywords: Macro-cell corrosion, Micro-cell corrosion, UPV test, Scanning Electron Microscopy (SEM).

1. INTRODUCTION

1.1 General

Concrete has become one of the most broadly used modern building materials, giving unmatched durability, strength, and flexibility in construction.[1] The incorporation of steel rebar inside concrete shapes a composite element, essentially enhancing its flexural capacity by checking the inherent tensile limitations of the cementitious concrete. [2] This made it possible to construct RC buildings like nuclear power plants, bridges, dams, etc. However, these sorts of materials degrade and ended up delicate over time. Rusting of the metal bars inside concrete can significantly weaken and shorten the life expectancy of concrete structures. It is a silent enemy that can wreak devastation on structures, economies, and human lives.

Corrosion is the damage emerging from the oxidation reaction between a metal or metal alloy and its surrounding environment. [3,4,5] It is an electrochemical process in which the concrete pore solution serves as the electrolyte, with dissolution of iron due to anodic reaction and reduction of oxygen due to cathodic reaction.[6] Aggressive agents, such as CO_2 and Cl^- penetrating the concrete up to the rebar are responsible for the development of this phenomenon.[7] Corrosion of steel can never be stopped in a natural environment without any protection. For reinforced concrete structures, the alkalinity of the pore solution and the protection from the cover concrete form a passivation film around the steel bars.[8] Primarily, the diffusion mechanism of corrosion develops in the exposed metal surfaces. Corrosion resistance of a material could be enhanced by decreasing the reactivity of the exposed surface i.e. passivation. [5][8]

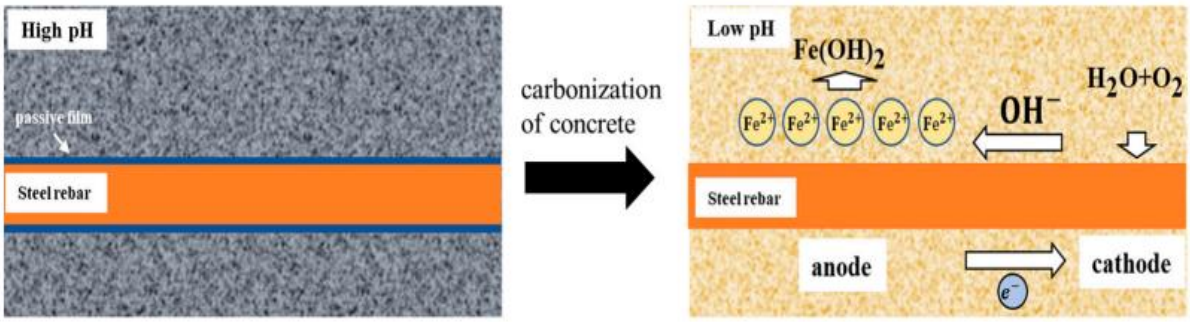

Figure 1: Corrosion mechanism of rebar initiated by the carbonization of concrete.[9]

1.2 Background

The concrete environment is highly alkaline, with a pH of almost 13, as a result of the cement hydration process, which produces a significant amount of OH^- ions. [9,10,11] Concrete being highly alkaline, the surface of steel rebar quickly forms a dense, protective film, providing the steel a passive state and preventing corrosion for a long time. [12,13,14,15] A passivation film with a thickness of 1~5 nm is developed in the steel surface in such alkaline environment. [16,17,18] In spite of that, corrosion of steel rebar can easily happen due to the external corrosive environment and defects of concrete materials.

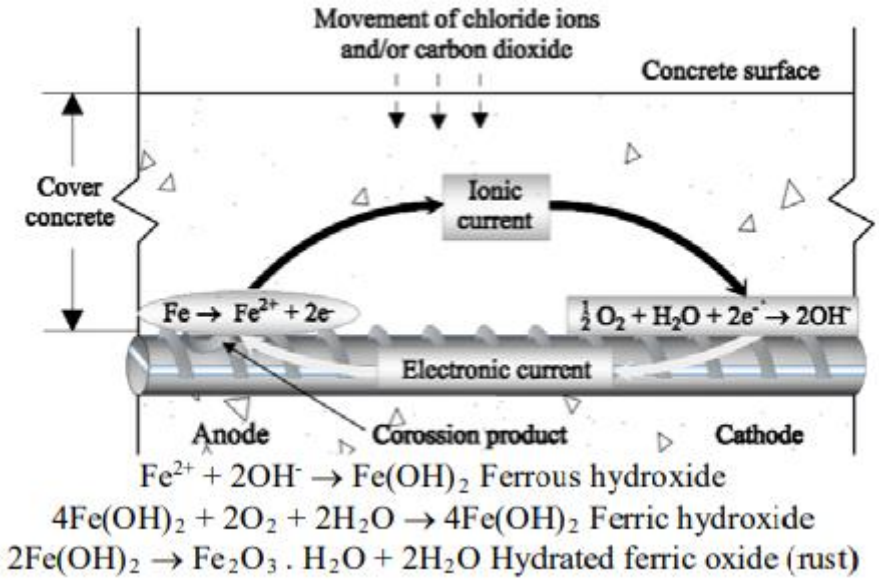

Figure 2: Component of corrosion reaction on rebar in concrete. [12]

Economic loss of around $2.5 trillion is originated by corrosion each year. [19] In the U.S., the direct cost of corrosion is about $276 billion annually, which is 3.1% of the 1998 GDP. Another study estimates that the U.S. faces corrosion-related damage worth $240 billion annually, where around 20% is attributed to the corrosion of reinforced concrete. [20]

Bangladesh's coastal regions are witnessing a surge in mega-projects, including marine infrastructure, tunnels, and seaports. These critical structures are inherently susceptible to corrosion, potentially leading to reduced durability, shortened service life, and increased maintenance costs. To ensure the long-term sustainability of these projects, effective strategies for mitigating corrosion in reinforced concrete structures are crucial.

Corrosion of the steel rebar will result from a number of components, including the diffusion of aggressive agent, such as chloride particles in the concrete pore structure, the reduced alkalinity of the passivation layer around the rebar concrete caused by carbonation, and the steel rebar's own insufficient corrosion resistance. Chloride induced corrosion being the most significant external factor leading to rebar corrosion, this research is based on the macro-cell and micro-cell corrosion of rebar in concrete due to inducing of chloride ion corrosion.

1.3 Scope:

This thesis investigates the combined effects of interfacial transition zones (ITZ) and chloride concentration on the corrosion behavior of steel bars in concrete. By employing various water-cement ratios to create different ITZ conditions around coated steel bars, the study will measure and compare both macro-cell and micro-cell corrosion under controlled chloride exposure. This research aims to elucidate the interplay between ITZ characteristics, chloride ingress, and the resulting corrosion processes, ultimately contributing to a better understanding of steel bar durability in reinforced concrete structures.

1.4 Research Flow

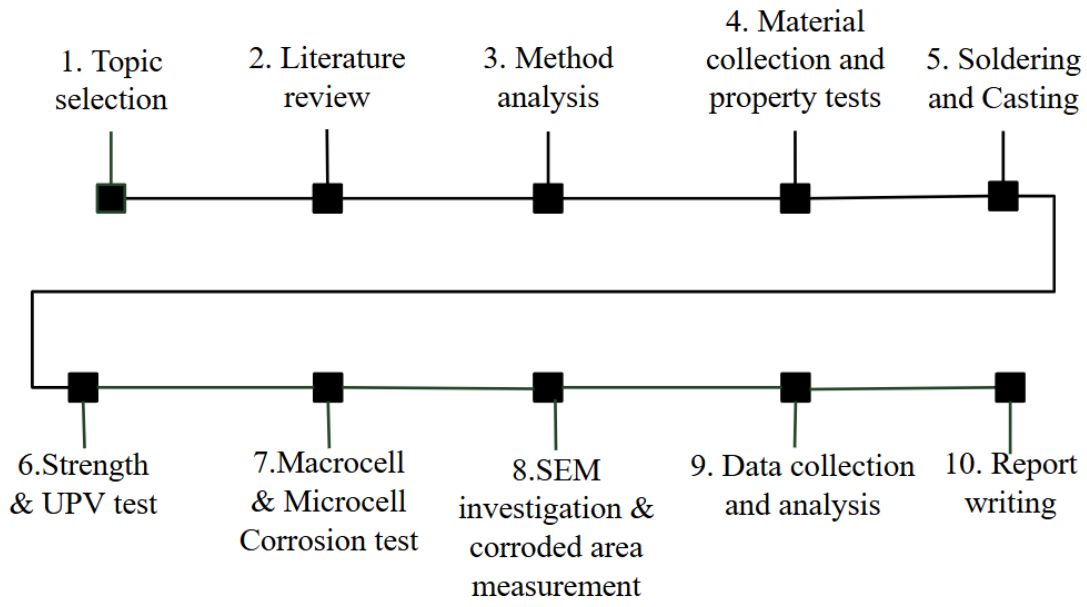

Figure 3: Research flow diagram

1.5 Layout of the Thesis

The thesis is organized as follows:

Chapter 1:

Introduction - This chapter delves into the theoretical foundation, historical context, research goals, and limitations of the study. It also visually presents the research process through a flowchart**.**

Chapter 2:

Literature Review - This chapter explores relevant research previously conducted in your field. It summarizes the findings of past authors to provide context for your own study.

Chapter 3:

Methodology - The methods and processes used to carry out our study are covered in this chapter.

Chapter 4:

Experimental Results and Discussion – Analysis and interpretation of the collected data and discussion are given in the chapter.

Chapter 5:

Conclusions and Recommendations - Suggestions and potential areas of future development are covered.

1.6 Research significance

While extensive research has investigated the corrosion of steel rebars in concrete for construction material durability and sustainability [30, 31], there is still much to learn about the impact of interfacial transition zones (ITZ) on corrosion. This study uniquely addresses this gap by examining the formation of ITZs using coated steel bars with varying water-cement ratios and both seawater and distilled water in the coating mix. We aim to measure and compare macro-cell and micro-cell corrosion of steel bars in these different ITZs, while also evaluating the impact of varying chloride concentrations on both types of corrosion.

2. LITERATURE REVIEW

Chloride-ion corrosion, a sort of typically localized corrosion, causes pitting corrosion of rebar in reinforced concrete structures working in chloride-containing environments, such as salt lakes and seas. The way that chloride ions influence the corrosion of rebar is mainly evident in the passive film's localized destruction [21]. Chloride ions have a very small diameter, allowing them to penetrate the passive film on the surface of rebar. When they adsorb and accumulate to a certain concentration, this leads to localized dissolution of the passive film and causes pitting corrosion of the rebar.

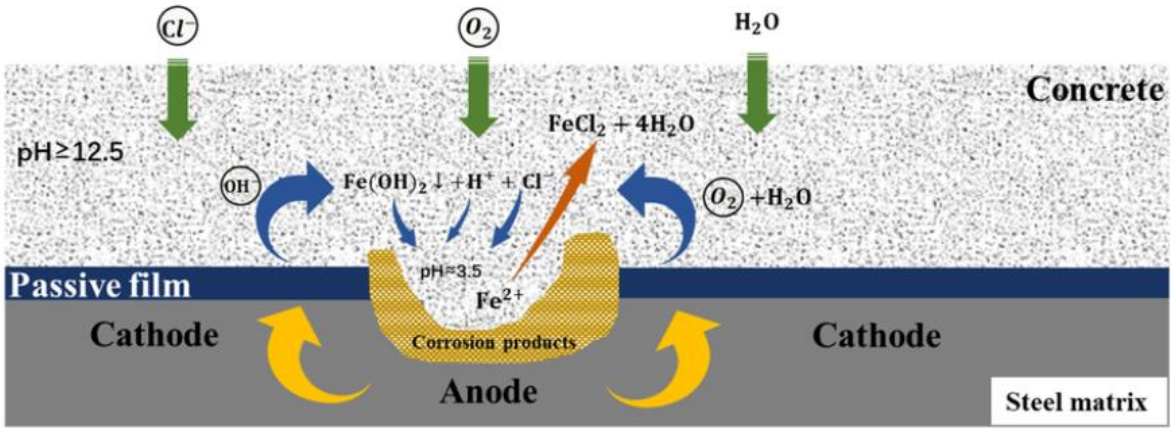

Figure 4: Rebar corrosion mechanism induced by the Cl- ions erosion. [9]

Macro-cell corrosion of steel rebar with a local anode and a local cathode is mostly caused by potential changes between various regions of the same rebar. The macro-cell corrodes at a faster rate the greater the potential difference. Macro-cell corrosion of steel is much more significant than micro-cell corrosion, because of its quick rate of corrosion, variety of forms, and reduction in corrosion. [22]

Macro-cell corrosion in reinforced concrete primarily occurs due to potential differences among rebars caused by environmental variations across different parts of the structure, as well as variations between different types of rebars. [22] In the macro-cell corrosion of rebar in concrete, anode is formed at part of the steel rebar with a lower potential. Cathode is formed at the part of the steel rebar with a higher potential.[23][24][25] Anodic rebar can corrode more quickly due to macro-cell corrosion, which can seriously harm reinforced concrete structures.

Since the damage caused by macro-cell corrosion is greater and more difficult to manage than that of micro-cell corrosion, further research and discussion are necessary.

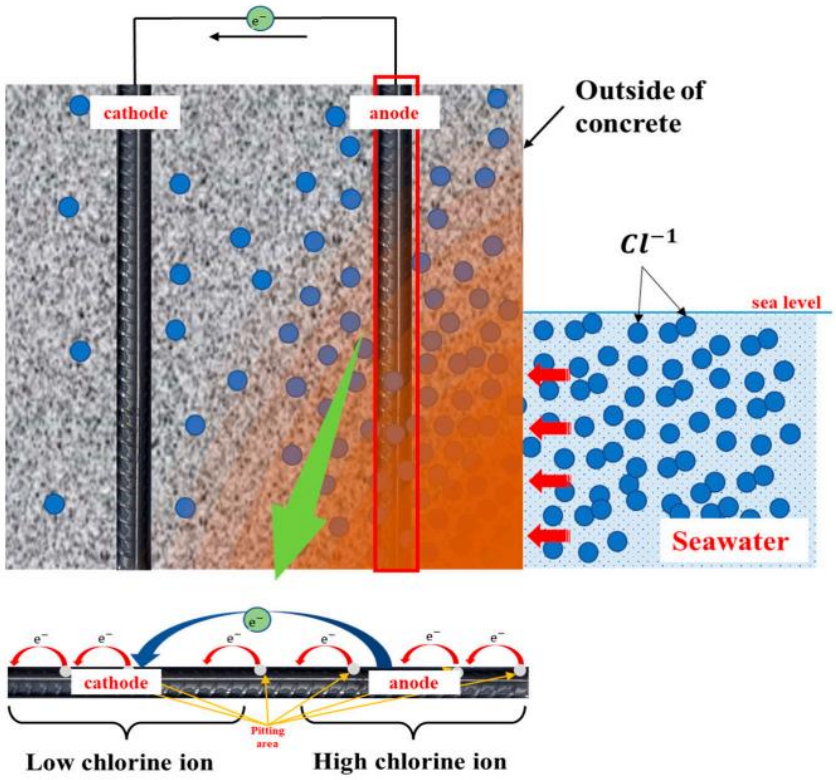

Figure 5: Schematic diagram of macro-cell corrosion of rebar induced by chloride-ion concentration difference. [9]

Anode and cathode pairs that are adjacent to each other cause micro-cell corrosion, which dissolves iron uniformly over the surface.

Uniform corrosion of steel rebar in concrete typically results from widespread carbonation of the concrete or uniformly high chloride concentrations near the steel. [26] In micro-cell corrosion, specific regions of the steel surface act as anodes, where oxidation reactions occur, and nearby regions act as cathodes, where reduction reactions take place. This creates an electrochemical gradient that speeds up the corrosion process in specific areas, leading to pitting, cracking, and overall deterioration of the steel reinforcement within the concrete structure.

To examine the possibility of chloride ingress into concrete, cylindrical specimens were submerged in seawater for 60 days at 40°C. Prism specimens with segmented steel bars were created to study macro-cell and micro-cell corrosion, half-cell potential, measurement of the corroded area, SEM investigation, and measurement of chloride concentration in the corroded area. Specimens were constructed using steel bars coated in epoxy. These specimens underwent **50 days** of exposure to a seawater splash environment. At appropriate intervals, measurements of the macro-cell corrosion current were conducted. Physical assessment of steel bar corrosion, including pit depths and corroded areas, was also conducted after the specimens were opened.

3. METHODOLOGY

3.1 Material properties

The construction used CEM Type III-B specified in BDS-EN-197-1-2003 with a slag content of 68% of the cement mass. The specific gravities of the cement were calculated using ASTM C188. Coarse aggregates were stone chips, and fine aggregates were natural river sand, with specific gravity, absorption, and fineness modulus of sand at 2.57, 2.59%, and 2.44, and for gravel at 2.66, 0.91%, and 6.66, respectively. The carbon, silicon, manganese, phosphorous, sulfur, and iron content in the steel bars were 0.22, 0.2, 0.65, 0.031, 0.031, and 98.868%, respectively. The maximum size of the coarse aggregate was maintained at 20 mm The chemical compositions of coarse aggregate, sand, and cement are given in Tables 1,2, and 3 respectively.

The minimum yield strength of the steel bars was 500 MPa, according to ASTM A706. For reinforcement, 10 mm diameter steel bars were used. Segmented steel bars (135 mm on both sides and 50 mm in the middle or cracked region) were used to monitor macro-cell corrosion. The segmented steel bars were isolated in the specimens, and the electrical connections were provided by using electrical wires from the outside. In addition to segmented steel bars, an isolated continuous steel bar was also provided at the same depth adjacent to the segmented bars. The chemical composition of steel rebars and their connection to the data logger are given in Table: 4 and Figure 6 respectively. Seawater from the Bay of Bengal was collected and used to mix the concrete and cement slurry which is used for coating.

Table 1 : Chemical composition of coarse aggregate

Coarse Aggregate		
Items	**Specification**	**Result**
Specific gravity	ASTM C127	2.66
Absorption capacity (%)	ASTM C127	0.91
Abrasion value (%)	ASTM C131	15.312
Unit weight (Kg/m^3)	ASTM C29	1575

Table 2 : Chemical composition of fine aggregate

Fine Aggregate		
Items	**Specification**	**Result**
Specific gravity	ASTM C127	2.57
Absorption capacity (%)	ASTM C127	2.59
Fineness Modulus (FM)	ASTM C136	2.44
Unit weight (Kg/m^3)	ASTM C29	1517

Table 3: Chemical composition of cement

Cement			
Type	Clinker (%)	Slag (%)	Gypsum (%)
CEM Type III-C	30	68	2

Table 4: Chemical composition of steel rebar

Steel Rebar						
Element	Fe	C	Mn	Si	S	P
Percentage (%)	98.868	0.22	0.65	0.2	0.031	0.031

Figure 6: Connection of rebars with data logger

3.2 Details of specimens and cases investigated

3.2.1 Cases Investigated

Ten different cases were investigated in total. For each case, one 100 mm × 100 mm × 400 mm prism specimen and three 100 mm × 200 mm cylinder specimens were prepared. In total, 10 prism specimens and 30 cylinders were prepared. Table 5 illustrates the mix proportions of concrete for respective cases with w/c ratio of 0.45 and s/a absolute volume ratio of 0.44. Cement content was 340 kg/m^3. There are three different types of seawater content. For cases one to seven and ten, the seawater chloride concentration was 12.7% of cement mass and for case 8, it was 0.4% of cement mass and lastly, the seawater chloride concentration for case nine was 0.2% of cement mass. We have maintained the seawater chlorine concentration by mixing seawater with distilled water in three different proportions. For the mixture of cement coating, we have used different water-cement ratios for different cases. For the cement-coating mixture, seawater has been used. The mix proportions of cement coating are summarized in table 6**.** In each prism specimen, one continuous steel bar and one segmented steel bar were placed.

Table 5: Cases investigated

Cases	Chloride Concentration	Coating over Steel Bar (w/c ratio)	Cement
1	12.7 % of cement mass	No Coating	CEM Type III-C
2		0.3	
3		0.4	
4		0.5	
5		0.6	
6		0.7	
7		0.8	
8	0.4% of cement mass	0.8	
9	0.2% cement mass	0.8	
10	12.7 % of cement mass	0.9	

Table 6: Mix design

W/C	S/A	Seawater Chloride Concentration	Plasticizer (4 ml/kg cement)	Cement (kg/m^3)	Sea Water (kg/m^3)	Distilled Water (kg/m^3)	Fine Aggregate (kg/m^3)	Coarse Aggregate (kg/m^3)
0.45	0.44	18200	4	340	153	-	806	1058
0.45	0.44	520	4	340	4.42	148.58	806	1058
0.45	0.44	260	4	340	2.21	150.79	806	1058

3.2.2 Details of specimens

The steel bars were cleansed with a 10% diammonium hydrogen citrate solution. The length of the continuous steel bar is 340 mm which was provided to prevent a collapse of the prism specimen. The segmented steel bar has three parts, two edge segments of 135 mm in length and 50 mm in length in the middle, which were used to measure the macro-cell and micro-cell corrosion current in different regions. The wires were connected by soldering. The orientation of the steel bars in the prism specimens is shown in figure 6. To provide electrical isolation inside the specimens the segmented steel bars were connected by epoxy. The segmented steel bars were electrically connected from the outside of the specimens by electrical wires. A 100-ohm resistor was placed to measure the voltage drop.

A data logger (TDS 150) was used to record the voltage drops at 90 predefined intervals. As the specimens were created using seawater in concrete mixing, macro-cell corrosion started right after the casting. The specimens were connected with the data logger immediately after casting to measure macro-cell corrosion current. The concrete covering had a thickness of 20 mm. Following casting, the prism specimens were allowed to cure for ninety days under wet jute bags that were securely sealed with polythene to keep moisture from escaping.

The specimens were fabricated with cement (W/C=0.45) paste-coated steel bars. After coating, the coated steel bars were cured for 24 hours. The coated bars and their connection with wires are shown in figure 7. The layouts of the specimens are shown in figure 8. The segmented steel

bars were electrically connected from the outside of the specimens by electrical wires. A 100-ohm resistor was placed to measure the voltage drop samples.

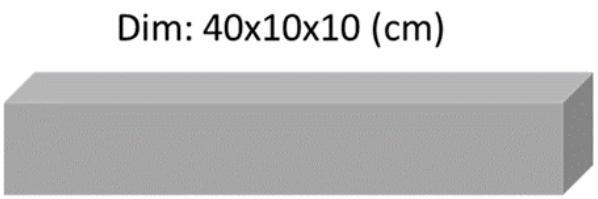

Specimen Dimensions

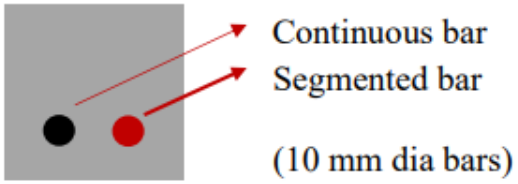

Cross sectional view of prism specimen

Figure 7: Prism specimen dimensions

Figure 8: Cement coated rebar and the connection of rebar and wires

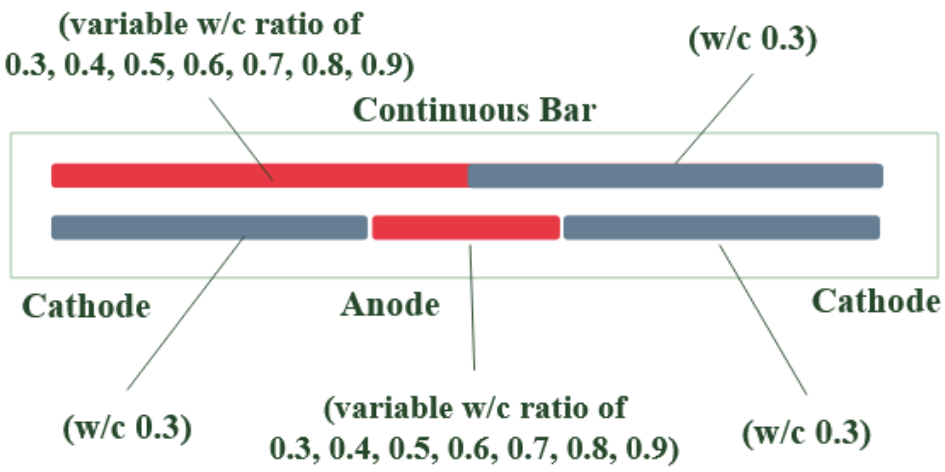

Figure 9: Layout of rebars in concrete specimen (prism)

3.3 Methods of evaluation

3.3.1 UPV test

The Ultrasonic Pulse Velocity (UPV) test is a nondestructive method for assessing the homogeneity, quality, cracks, and internal flaws in concrete. We have used an ultrasonic pulse velocity tester to understand the concrete quality using ASTM C597.

Figure 10: UPV test

3.3.2 Compressive strength

The concrete's compressive strength of ASTM C39 was used to measure the cylinder specimens. We measured the compressive strength of the cylinder specimens (100 mm in diameter and 200 mm in height) after 7 days, 28 days, 56 days, and 90 days.

Figure 11: Compressive strength test

3.3.3 Chloride ingress in concrete

For the development of macro-cell corrosion, one of the most critical influencing elements is the chloride content. Following a 3-month curing period under moist jute cloths, the prism specimens were immersed in seawater for 60 days at 40°C in order to measure the chloride profiles in the concrete at various ages of exposure to warm salt water. After exposure to salt water for 120 and 180 days, chloride profiles were measured. To measure the amount of water-soluble chloride in concrete, a 100 mm-high disc was cut out of the center of each specimen. In order to gather concrete samples from the specimens at 10–20 mm from the steel cover to

the center region of the specimens, the discs were cut again. We have collected concrete samples for each case from both the cathodic and anodic region.

The samples of concrete were ground into a powder and put through a #50 sieve to determine the water-soluble chloride content in the concrete. Chloride concentrations around steel bars at the middle bar (anode) and edge bar (cathode) were measured after electrochemical investigation. The concentration of water-soluble chloride in the powder samples was determined using JCI SC4.

3.3.4 Macro-cell corrosion

Macro-cell corrosion is typically found where the critical chloride content has been reached and consists of spatially isolated anodes and cathodes. A data logger was utilized to measure the potential drop between the steel segments which was connected to the specimens during the casting process. The equipment is permanently set up for 30 days and can be used to monitor the potential drop with pre-fixed intervals of time between steel elements in segmented steel bars. The connection and setup of the data logger is presented in Figure 6. The current flow from the measured voltage drop through a fixed resistance of 100 Ω was computed using the following equation.

$$I = \frac{V}{R} \tag{1}$$

Where, I = Current (Ampere) V = Voltage drop R = Resistance (100 Ω). The macro-cell corrosion current density was determined by utilizing the subsequent equation:

$$I_{mac} = \frac{I}{A} \times 10^{6} \tag{2}$$

where A is the surface area of the steel segment in cm^2, I is the current and I_{mac} is the macro-cell corrosion current density in $\mu A/cm^2$.

3.3.5 Micro-cell corrosion

In an initial experiment, a steel structure was placed in a highly humid environment (99% humidity) at a cool temperature of 20°C. As expected, no corrosion was observed. The experiment then continued by subjecting the structure to a simulated wet-dry cycle: it was sprayed with water once daily for 5 minutes while maintaining the high humidity of 99%. Interestingly, even when the temperature was subsequently increased to 40°C and the wet-dry cycle continued, only minimal signs of corrosion were detected. This suggests that temperature alone, even at a moderate 40°C, might play a minor role in initiating corrosion in a highly humid environment for steel structures, especially when the wetting duration is limited.

The scenario changed significantly when the steel structure was submerged in seawater of Bay of Bengal at 40°C. In this scenario, corrosion readily occurred, and the specific type identified was microcell corrosion. This highlights the critical role of electrolytes (salts found in seawater) in triggering and accelerating the corrosion process.

The micro-cell current density was computed using the subsequent formula.

$$I_{mic} = \frac{B}{R_P} \times 10^6 \tag{3}$$

Here, I_{mic} is the micro-cell current density in μA/cm^2 and Rp is the polarization resistance in Ω·cm^2.

$$B = \frac{\beta_a \beta_c}{2.3(\beta_a + \beta_c)} \tag{4}$$

Here, B depends on the slopes of the anodic (βa) and cathodic (βc) polarization curves. The value of B is considered to be 0.026 V.

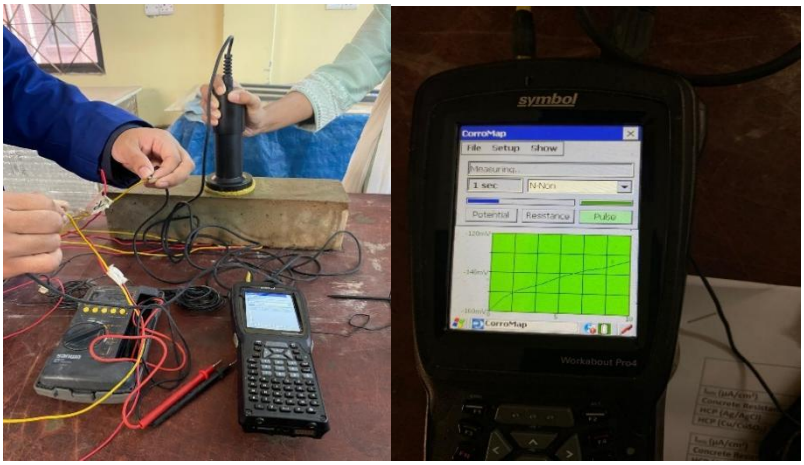

Figure 12: Measuring the microcell corrosion using corro-map machine.

3.3.6 Depth of corrosion

The depth of corrosion over the steel bars was calculated by using the following equation 5 and 6.

$$D = 0.0116 \times I_{mac} \times t \quad (5)$$

Where D denotes the depth of corrosion in mm, I_{mac} denotes the macro-cell corrosion current density in μA/cm^2, and t is time in years.

$$I_{avg} = I_{mac(avg)} + I_{mic(avg)} \quad (6)$$

$I_{mac(avg)}$ was calculated by integrating the macro-cell corrosion values and the dividing it by the total exposure time.

$I_{mic(avg)}$ is the average of micro-cell corrosion before and after the exposure at the middle segment of the steel bar.

3.3.7 Half-cell potential

To prevent constructions in the macro-cell corrosion current flow, half-cell potential is measured. When determining the potential of a particular segment, the section of steel that was electrically isolated from the rest of the segment. According to ASTM C876, the corrosion probability for various half-cell potential (Ag/ AgCl) values was calculated.

3.3.8 Concrete resistance

Concrete resistance, encompassing its ability to resist factors like weather, chemicals, and corrosion, is a critical property measured to ensure the durability and longevity of concrete structures. The concrete resistance over the steel bar was calculated using a portable corrosion monitoring device.

3.3.9 Visual observation and measurement of corroded area

After electrochemical analysis, the prism specimens were split open. The anode and cathode bars were then separated from the specimens to visually inspect and measure the corrosion area and pit depth. On a clear sheet of paper, the rusted area above the steel bars was sketched, and the area was then measured. Nails were inserted into the corrosion pits to determine the depth of the corrosion, if any.

3.3.10 Scanning Electron Microscope

In this investigation, a multifaceted approach was employed to characterize the coating on steel rebars embedded within a concrete matrix. The initial phase involved the utilization of a Scanning Electron Microscope (SEM) to meticulously examine the coating and ascertain its thickness. Subsequently, concrete samples containing the rebars were fractured along their longitudinal axis, exposing the interfacial region between the concrete and the steel. This facilitated the observation of any potential deposits that might have accumulated in the vicinity of the anode and cathode of the rebar within the concrete matrix. To enhance the efficacy of the SEM analysis, the fractured surfaces were then meticulously coated with a thin layer of gold. This improved the electrical conductivity of the sample surface, yielding superior-quality SEM images. Finally, energy-dispersive X-ray (EDX) analysis was performed to meticulously

identify the elemental composition of the deposits observed on the fractured surfaces. In essence, this comprehensive methodology enabled a thorough investigation of the coating on the steel rebars, the potential deposition phenomena occurring at the anode and cathode interfaces within the concrete, and the elemental composition of any deposits formed in these regions.

4.RESULTS AND DISCUSSIONS

4.1 UPV test of concrete

Table 7: Concrete quality with respect to pulse velocity [33]

Pulse Velocity	Concrete Quality
>4000 m/s	Very good to excellent
3500-4000 m/s	Good to very good, slight porosity may exist
3000-3500 m/s	Satisfactory but loss of integrity is suspected
<3000 m/s	Poor and loss of integrity exists

The UPV of concrete at 7 days, 28 days, 56 days, and 90 days was determined and shown in Fig. While the results might show a slight initial increase in UPV with higher chloride content due to accelerated early hydration, this is likely followed by a later decrease in UPV. This is because the formation of CaCl2 from seawater chlorides can contribute to increased porosity and potential micro-cracking within the concrete over time. These factors can lead to faster chloride ion penetration and potentially accelerate steel corrosion, ultimately increasing UPV. As the all values of UPV test are greater than 3500 m/s, so concrete quality is very good.

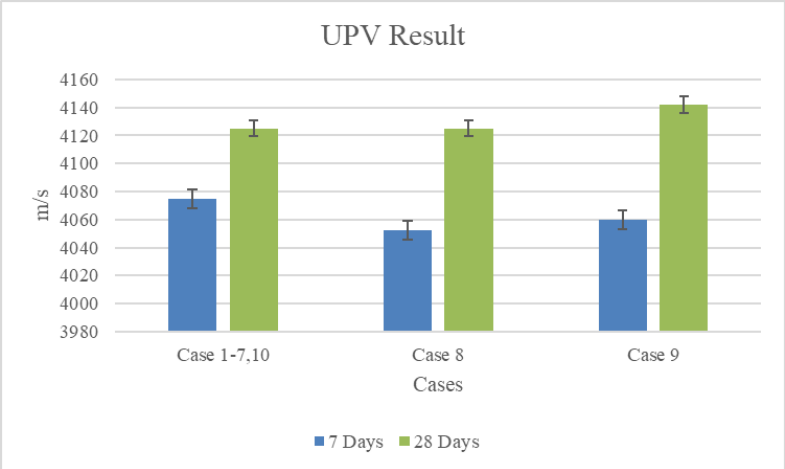

Figure 13: Result of UPV test

4.2 Compressive Strength of Concrete

The compressive strength of concrete at 7 days, 28 days, 56 days, and 90 days was determined and shown in figure 14. From the test result, it is visible that the compressive strength is higher in cases with lower chloride content. As the Chlorine in seawater forms $CaCl_2$, it accelerates the hydration of C3S. As a result, the early strength of concrete is higher with more chloride-content mixture.

Seawater mixed concrete with higher chloride content showed higher compressive strength after 7 days. But later it has one serious effect on the concrete which is the corrosion of steel with eventually.

Compressive strength of seawater-mixed concrete increases regardless of the curing temperature. The strength gain observed rapid acceleration during the initial curing days (1 and 3 days) and seems to slow down with extended curing periods (7 and 28 days**).**

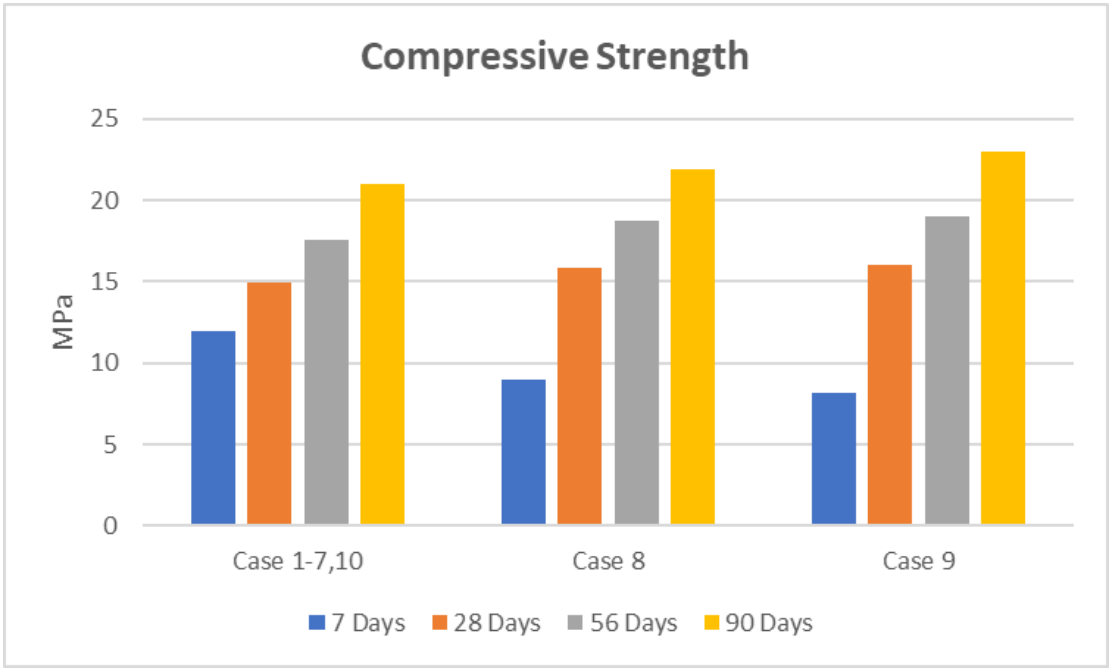

Figure 14: Result of compressive strength

4.3 Chloride ingress in concrete

Considering chloride concentrations of case 2 and case 10, initially the percentages of cement mass were high. After the crushing of specimens as powder, the chloride concentration reduced but higher than the threshold limit of chloride against corrosion of steel in concrete (0.4% mass of cement mass). [34]

The reason can be the mixing of cement coating, aggregates with the powdered specimens. For case 8, initial value of chloride concentration was equal to the threshold limit but the final value reduced a bit than the initial value. For case 9, the chloride concentration was half of the threshold limit, although there was little bit corrosion on the steel bar. Therefore, micro-level corrosion was observed in spite of less amount of chloride concentration.

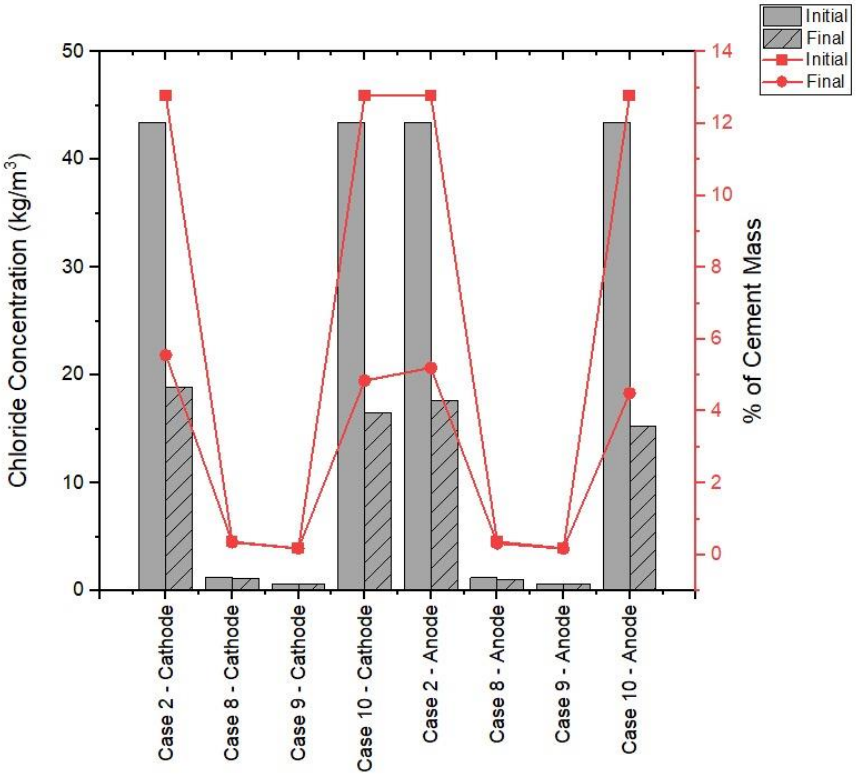

Figure 15: Analysis of chloride concentration along the steel bar

4.4 Macro-cell corrosion current density (I_{mac})

Macro-cell corrosion was found to be dependent on the rebar potential difference, with coated rebars exhibiting lower corrosion rates. Macro-cell corrosion current density measured at the ages of 30 days is shown in figure 16 for different types of specimens. The segmented middle steel bars seem to be anodic with respect to the segmented edge bars. The largest macro-cell current density was found in case 10 which had the maximum porosity in ITZ (coating W/C ratio= 0.9) and maximum chloride concentration (12.7 % of cement mass). The increased porosity in the interfacial transition zone (ITZ) causes higher macro-cell corrosion current density. The smaller macro-cell corrosion current density was shown in case 2 which had the minimum porosity in ITZ (coating W/C ratio 0.3).

Among specimens with identical porosity in ITZ (W/C ratio= 0.8) but different chloride concentrations the smaller macro-cell corrosion current density was shown from the specimen having 0.2% of cement mass. The macro-cell corrosion current density exhibited a negative correlation with chloride concentration. This confirms that lower chloride concentrations lead to decreased corrosion.

Initially, seawater splashes cause a surge in macro-cell corrosion on the exposed specimens. However, this rate diminishes over time until the next exposure event. While the macro-cell corrosion rate fluctuates, it shows a general downward trend over time. To improve the performance of concrete using seawater, two approaches are possible:

1. **Reduce porosity of coating:** This can be achieved by lowering the water-to-cement ratio (W/C) and increasing the cement content. A denser cover allows less chloride ingress, thereby mitigating corrosion. [34]

2. **Dilute seawater with fresh water:** Mixing seawater with distilled water reduces the chloride concentration in the mix. However, the impact on strength needs to be considered.

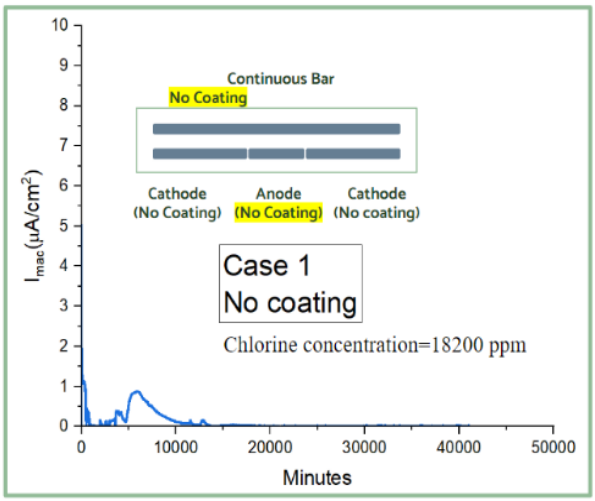
Continuous Bar
No Coating
Cathode (No Coating)
Anode (No Coating)
Cathode (No coating)
Case 1
No coating
Chlorine concentration=18200 ppm
I_{mac} (μA/cm^2)
Minutes

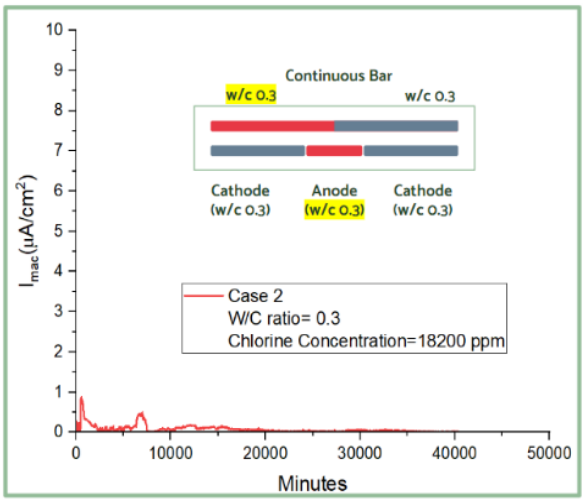
Continuous Bar
w/c 0.3
w/c 0.3
Cathode (w/c 0.3)
Anode (w/c 0.3)
Cathode (w/c 0.3)
Case 2
W/C ratio= 0.3
Chlorine Concentration=18200 ppm
I_{mac} (μA/cm^2)
Minutes

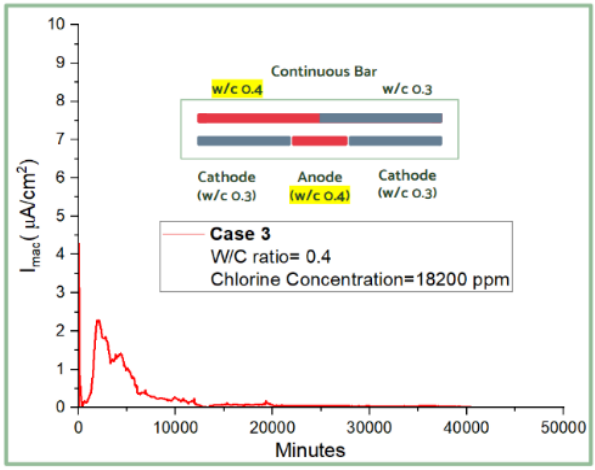
Continuous Bar
w/c 0.4
w/c 0.3
Cathode (w/c 0.3)
Anode (w/c 0.4)
Cathode (w/c 0.3)
Case 3
W/C ratio= 0.4
Chlorine Concentration=18200 ppm
I_{mac} (μA/cm^2)
Minutes

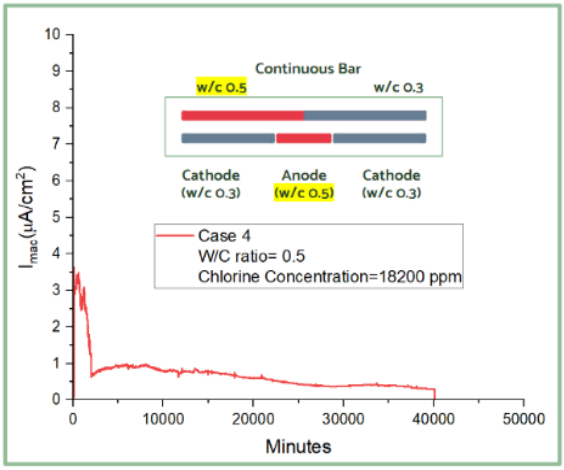
Continuous Bar
w/c 0.5
w/c 0.3
Cathode (w/c 0.3)
Anode (w/c 0.5)
Cathode (w/c 0.3)
Case 4
W/C ratio= 0.5
Chlorine Concentration=18200 ppm
I_{mac} (μA/cm^2)
Minutes

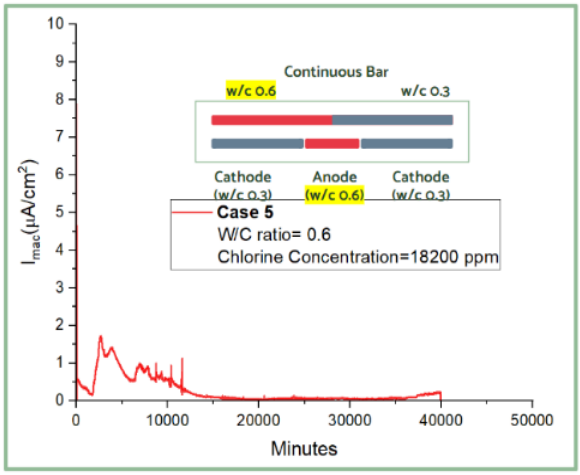
Continuous Bar
w/c 0.6
w/c 0.3
Cathode (w/c 0.3)
Anode (w/c 0.6)
Cathode (w/c 0.3)
Case 5
W/C ratio= 0.6
Chlorine Concentration=18200 ppm
I_{mac} (μA/cm^2)
Minutes

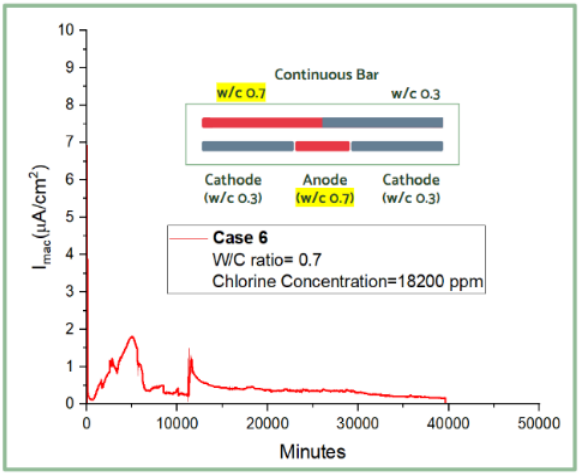
Continuous Bar
w/c 0.7
w/c 0.3
Cathode (w/c 0.3)
Anode (w/c 0.7)
Cathode (w/c 0.3)
Case 6
W/C ratio= 0.7
Chlorine Concentration=18200 ppm
I_{mac} (μA/cm^2)
Minutes

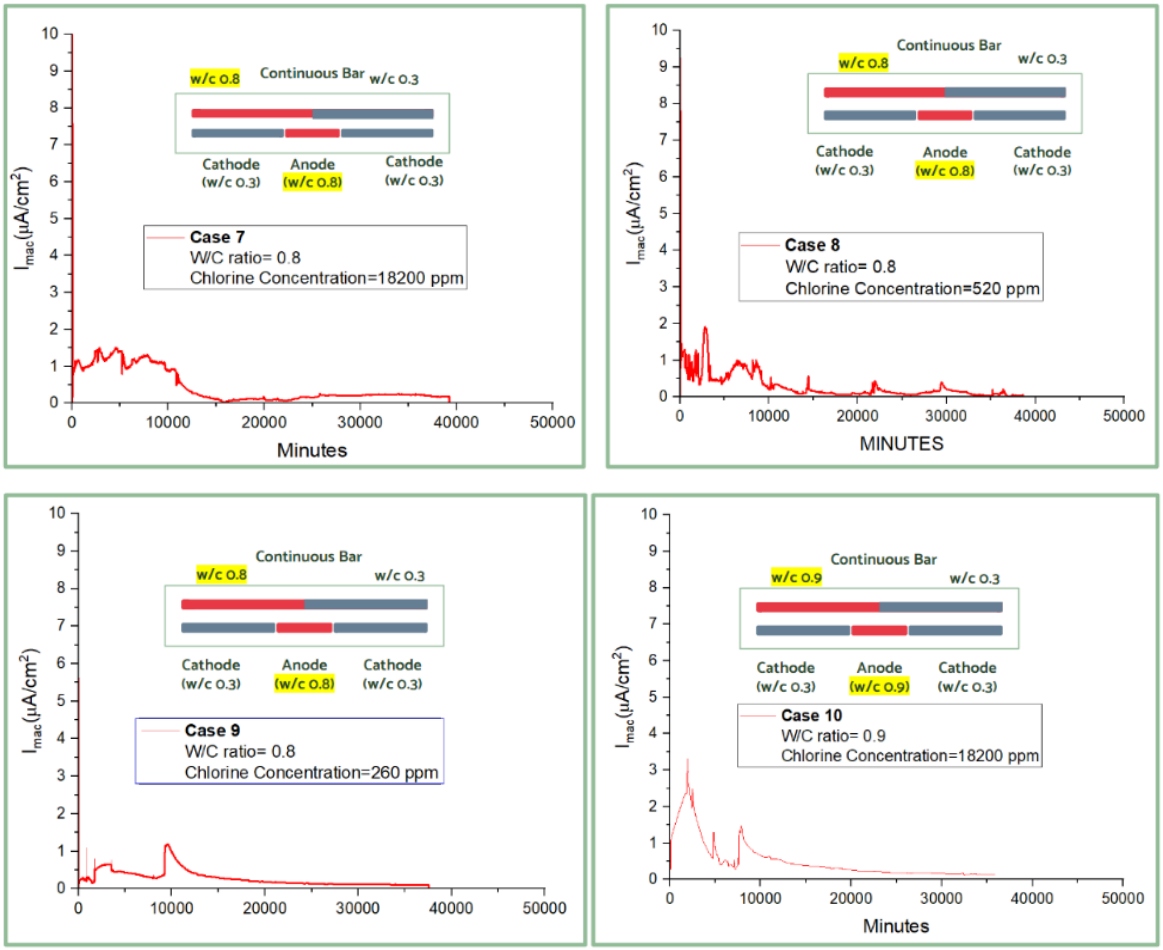

Figure 16: Measurement of macro-cell corrosion

4.6 Depth of Corrosion

To facilitate a more comprehensive comparison of the corrosion of the specimens, the areas under the macro-cell corrosion current density curves presented in Figure 16 were calculated. This data allows for a quantitative assessment of the macro-cell. The results are summarized in Figure 17. It is important to acknowledge that the actual corrosion depth can be significantly higher (ranging from four to eight times greater) than the calculated depth based solely on corrosion current data, as referenced in [37].

The results indicate the most pronounced corrosion activity for steel bars embedded in concrete containing the maximum amount of chloride content in the coating and maximum porosity in the ITZ. Consistent with the trends observed for macro-cell corrosion, the depth of corrosion increased with a higher water-cement ratio. Notably, Cases 8 and 9, which possessed the lowest

chloride concentration (0.4% of cement content and 0.2% of cement content respectively) among specimens with identical ITZ porosity, exhibited the lowest corrosion depths.

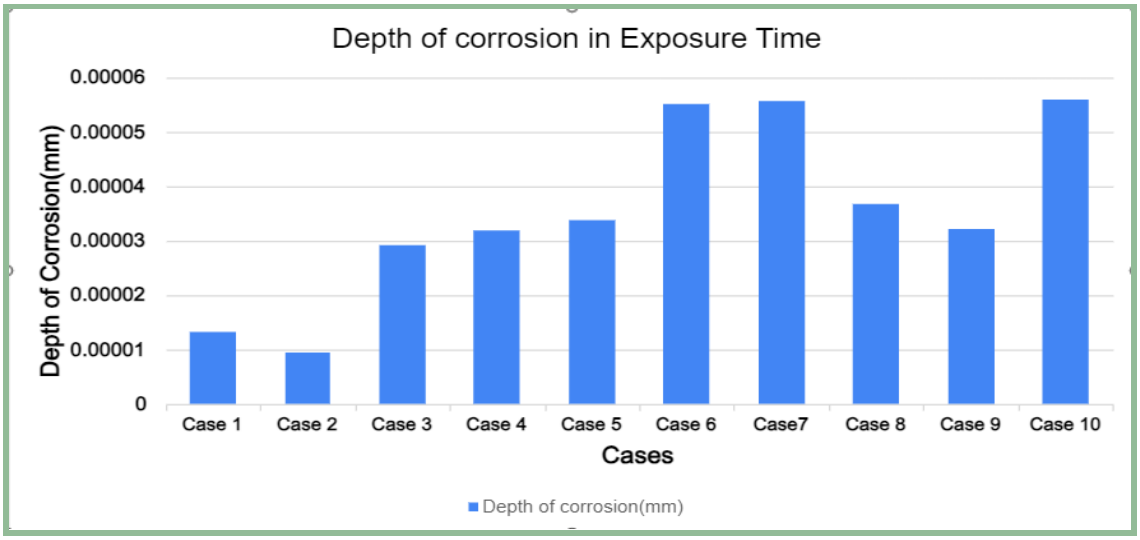

Figure 17: Measurement of depth of corrosion

4.5 Micro-cell corrosion current

Micro-cell corrosion analysis focused on the segmented middle bar, acting as both an anode and cathode. This investigation employed a corro-map machine to assess micro-cell corrosion within the steel bars. Table 10 presents the micro-cell corrosion current densities (Imic) measured before and after exposure to seawater. Notably, all specimens exhibited micro-cell corrosion current densities below 0.5 µA/cm² prior to seawater exposure. However, following exposure, most cases displayed a significant increase in corrosion current density, surpassing the 0.5 µA/cm² threshold. Specimens were submerged in seawater for 42 days within a humidity chamber, with micro-cell corrosion measured at 7-day intervals (7, 21, and 42 days). The results revealed a direct correlation between micro-cell corrosion current and the porosity of the interfacial transition zone (ITZ). Case 2 exhibited the lowest micro-cell corrosion, while Case 10 displayed the highest, aligning with their respective ITZ porosities. Interestingly, micro-cell corrosion exhibited a trend of increasing over time, contrasting with the observed decrease in macro-cell corrosion. This finding aligns with the results reported in a previous study [35].

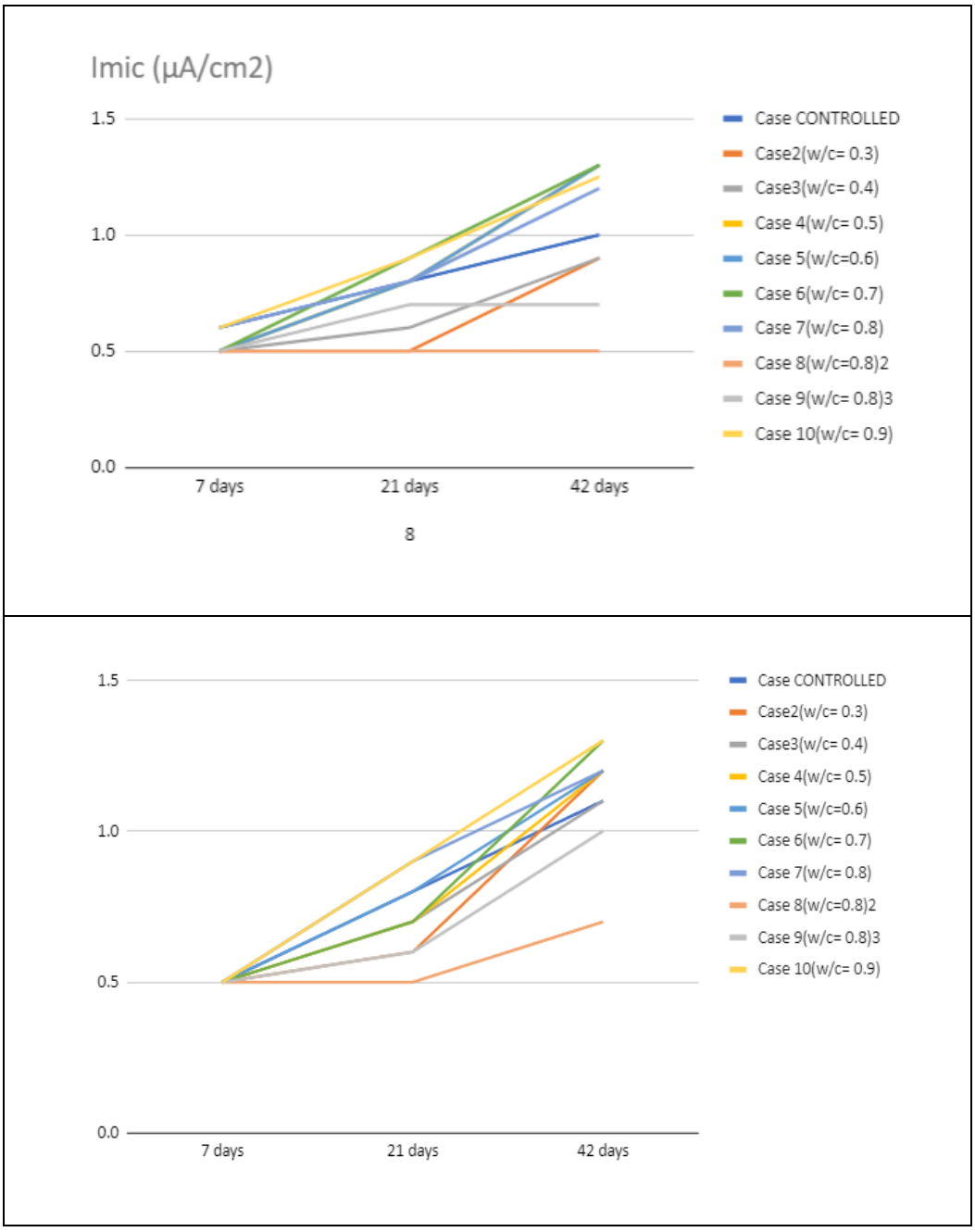

Figure 18: Measurement of micro-cell corrosion

Table 8 : Corrosion state with respect to corrosion current density [36]

Corrosion Current Density $i_{corr}\ (\mu A/cm^2)$	Corrosion State
<0.1	Passive
0.1-0.5	Low corrosion
0.5-1.0	Moderate
>1.0	High corrosion

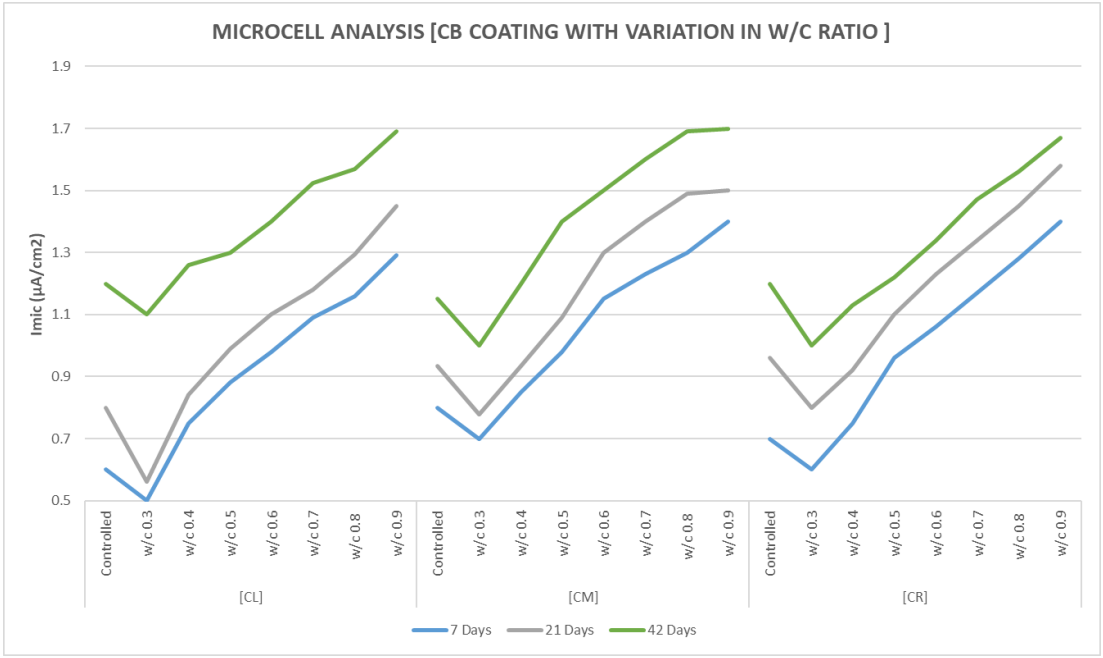

Figure 19: Micro-cell corrosion analysis for continuous bar having coating with different w/c ratio

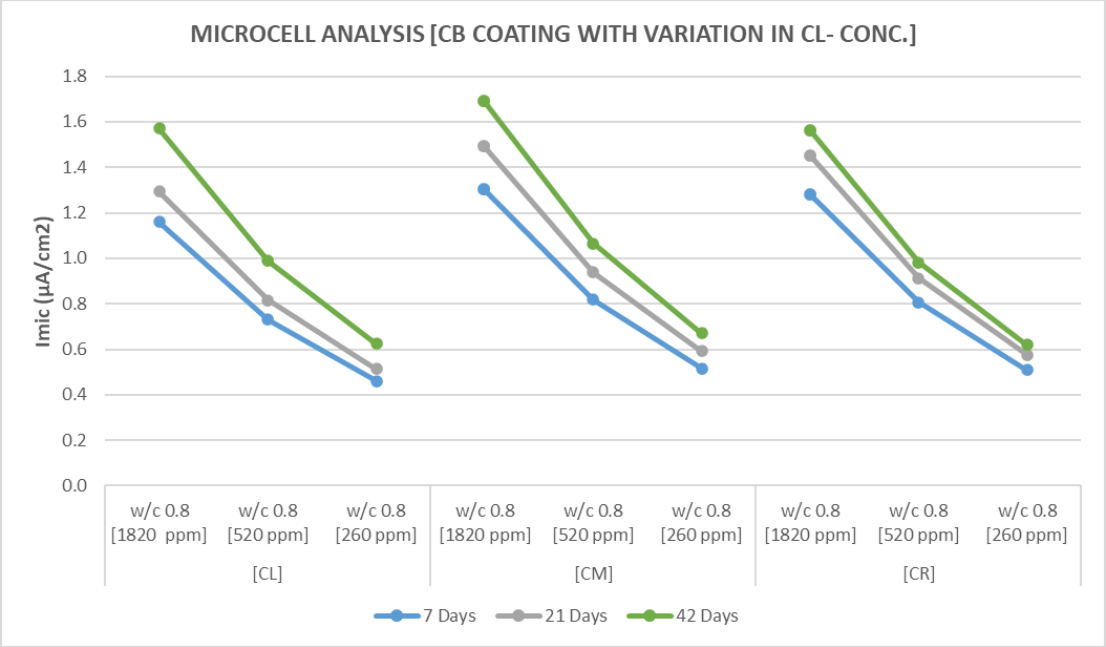

Figure 20: Micro-cell corrosion analysis for continuous bar having coating with different chloride concentration

4.8 Half-cell potential

Galvanic corrosion arises when two dissimilar metals or regions within a single material exhibit varying electrical potentials. This potential difference induces the flow of an electrical current between them, ultimately leading to the degradation of the material. Half-cell potential measurements confirmed the segmented middle bar acting as the anode due to its lower potential compared to the right and left bars. This suggests the formation of a weaker interface at the middle bar, promoting its corrosion activity, while denser interfaces formed on the right and left bars, acting as cathodes. From the results, it can be found that HCP values after exposure are increased significantly compared to the HCP values before exposure. These findings highlight the detrimental effect of ITZ porosity on micro-cell corrosion susceptibility and emphasize the importance of optimizing concrete mix design and curing practices to minimize ITZ porosity and enhance concrete durability in marine environments.

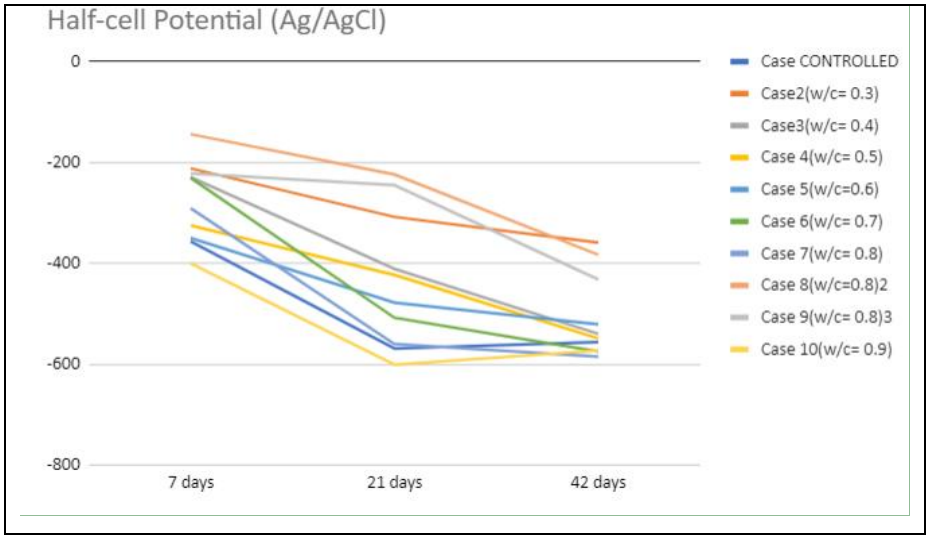

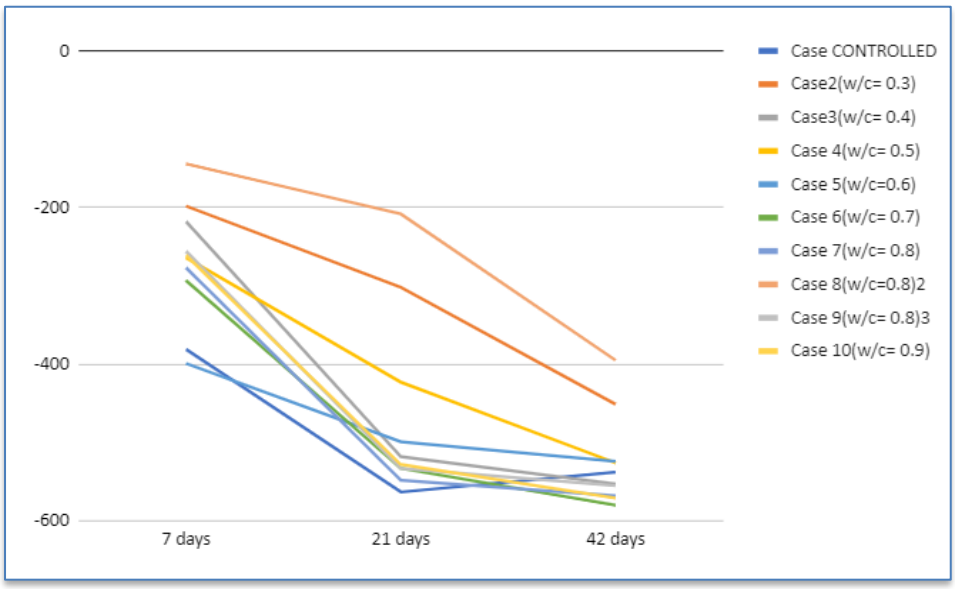

Figure 21: Measurement of half-cell potential

4.9 Concrete resistance

Measuring concrete resistance ensures safe, durable, and cost-effective structures by predicting longevity, preventing corrosion, optimizing mix design, and monitoring deterioration. The study observed a direct correlation between increased micro-cell corrosion current (indicating higher corrosion activity) and the porosity of the concrete's interfacial transition zone (ITZ). This suggests that denser concrete with a less porous ITZ offers greater resistance to micro-cell corrosion. This aligns with the concept of concrete resistance, where a more robust concrete

matrix provides a better barrier against corrosion-inducing agents, ultimately protecting the embedded steel. Interestingly, the observed increase in micro-cell corrosion over time suggests a potential future decrease in concrete resistance.

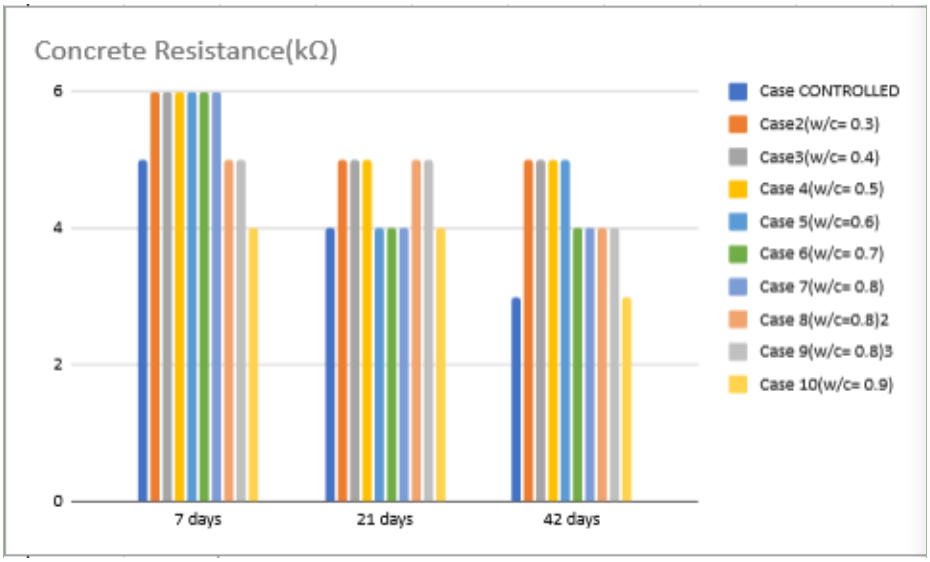

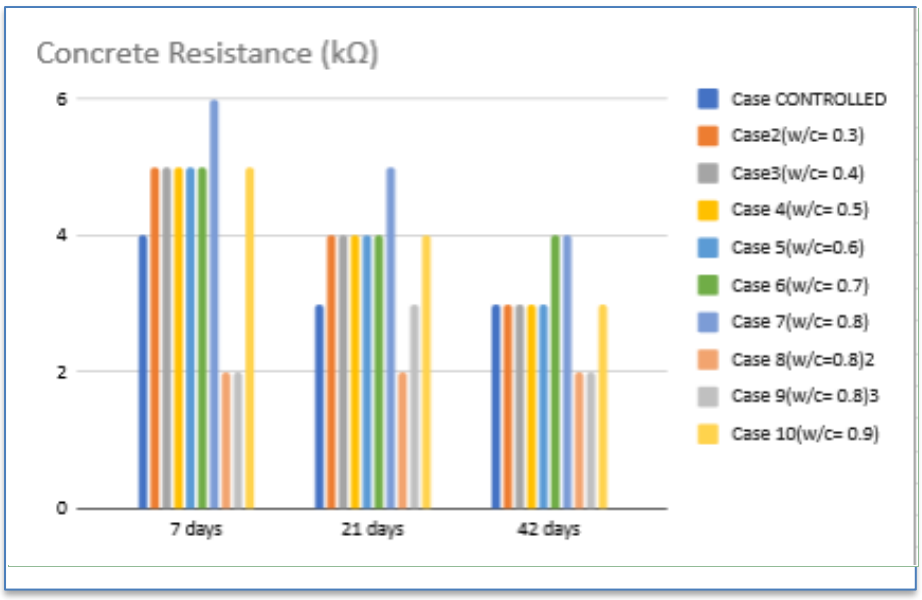

Figure 22: Measurement of concrete resistance

4.10 Corroded area

Following the completion of electrochemical investigations, the specimens were fractured, and the steel bars were extracted for visual inspection of rust formation. The surface conditions of steel bars are shown in fig. With the increase of water to cement ratio, the corroded area in the steel bars increased. Again, with the decrease of seawater concentration, rust formation over the steel bars drastically decreased. Maximum corroded area was found in case 10 which had the maximum porosity in ITZ (W/C ratio of coating = 0.9) and maximum chloride concentration (12.7 % of cement mass). On the contrary, negligible corroded area was found in densely coated steel bar which is case 2 (W/C ratio of coating = 0.3). Higher amount of corroded area was found in segmented middle steel bar due to high cathode to anode ratio.

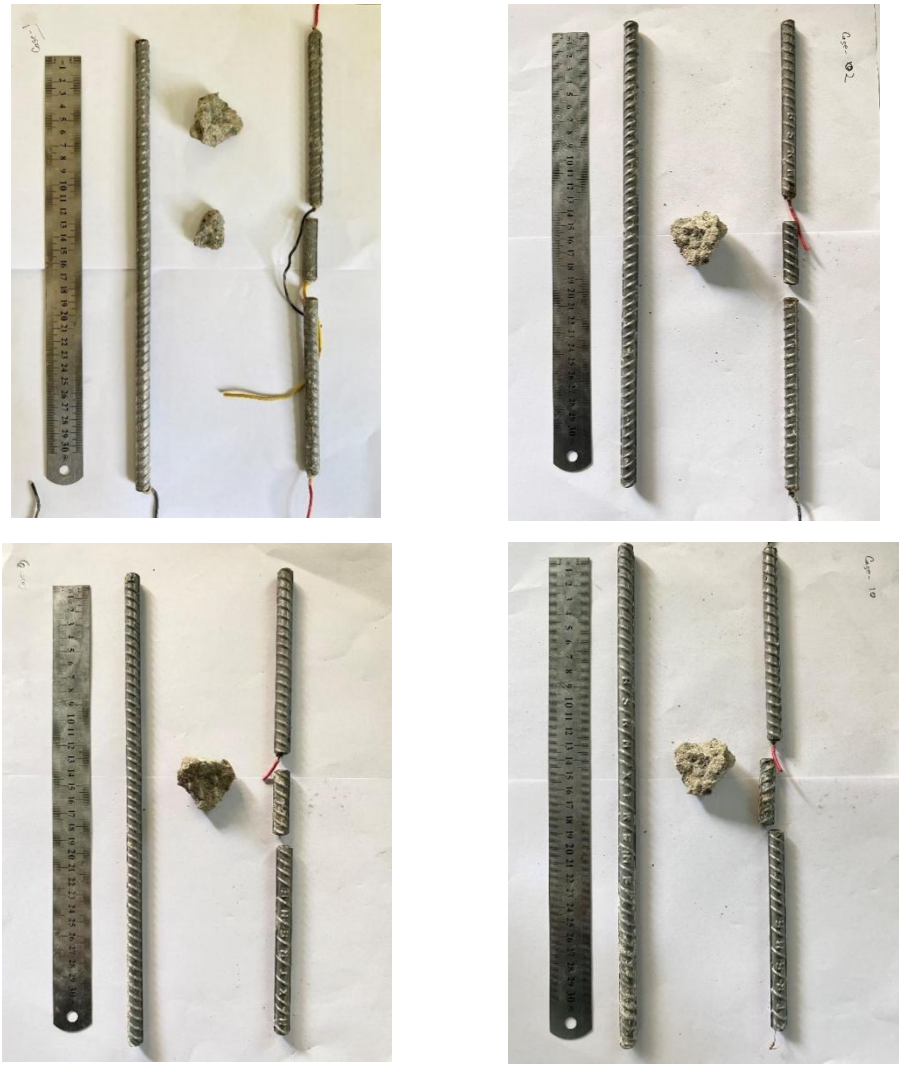

Figure 23: Visual observation of continuous and segmented steel bars; (a) case 1; (b) case 2; (c) case 9; (d) case 10

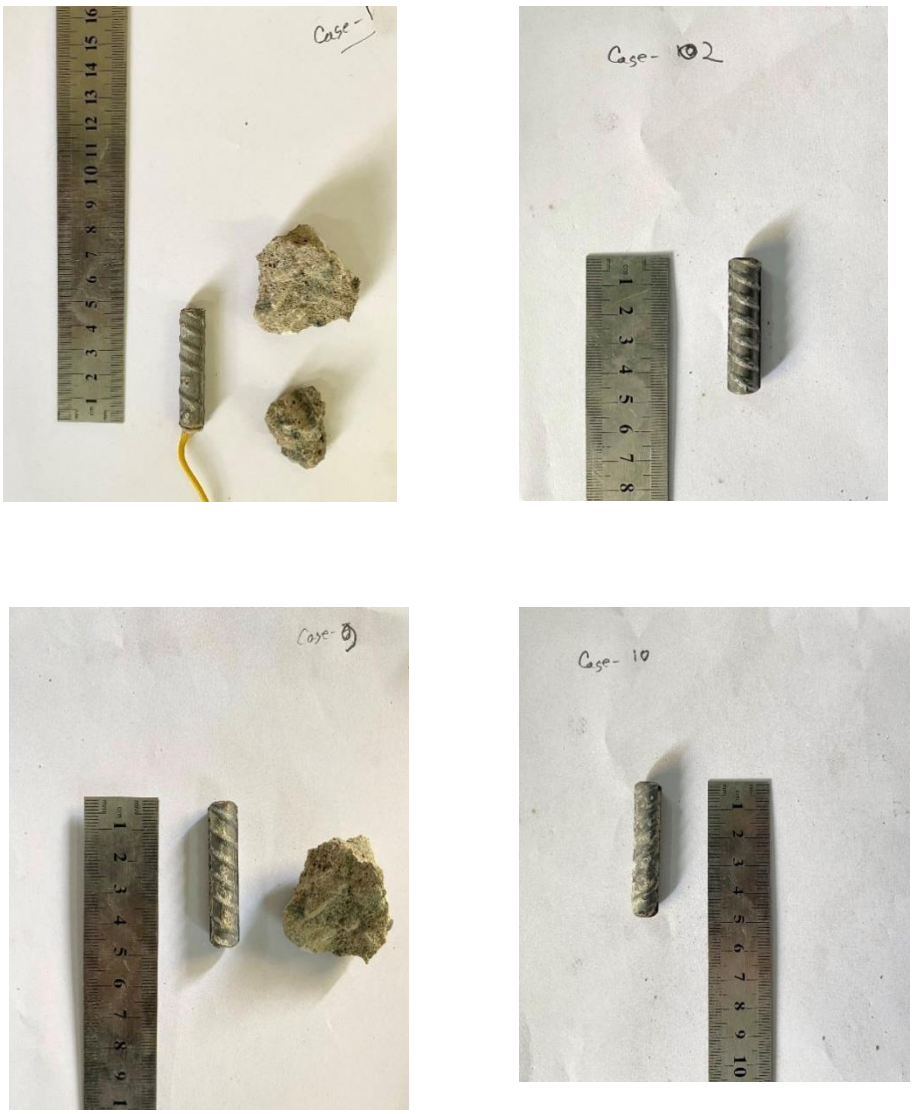

Figure 24: Visual observation of segmented middle steel bar; (a) case 1; (b) case 2; (c) case 9; (d) case 10

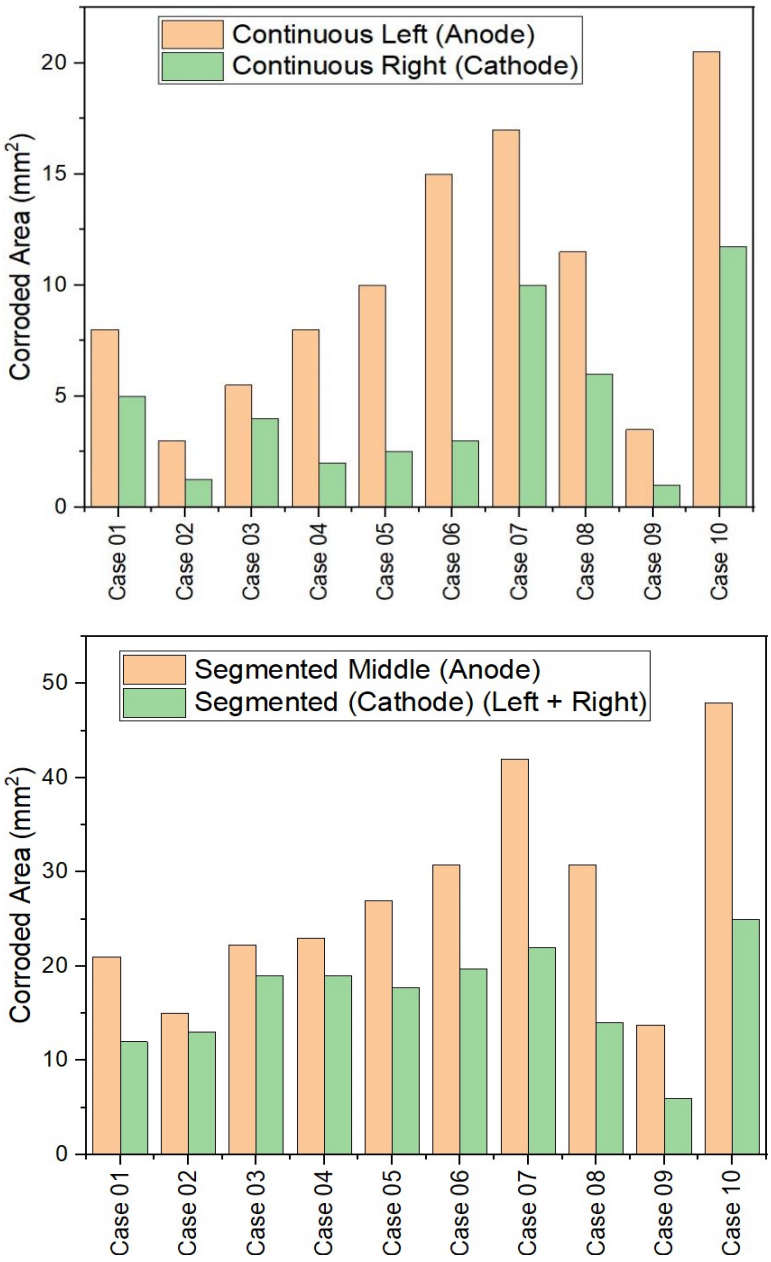

Figure 25: Measurement of corroded area

4.11 Microscopic investigation by SEM

The Scanning Electron Microscope investigation found more voids when the coatings had higher water-to-cement ratios. After the investigation using energy-dispersive X-ray, rust was found in the steel and cement coating interface. Some depositions of needle crystals of ettringite, calcium hydride, and calcium monohydride crystal structures were found, which helped to heal the interface's void and thus reduced the macro-cell corrosion. In Figure 24, detailed pictures were given where the void is more evident for higher water-to-cement ratios and less void for lower water-to-cement ratios. Some spherical lump-shaped fly ashes were also found in the SEM investigation.

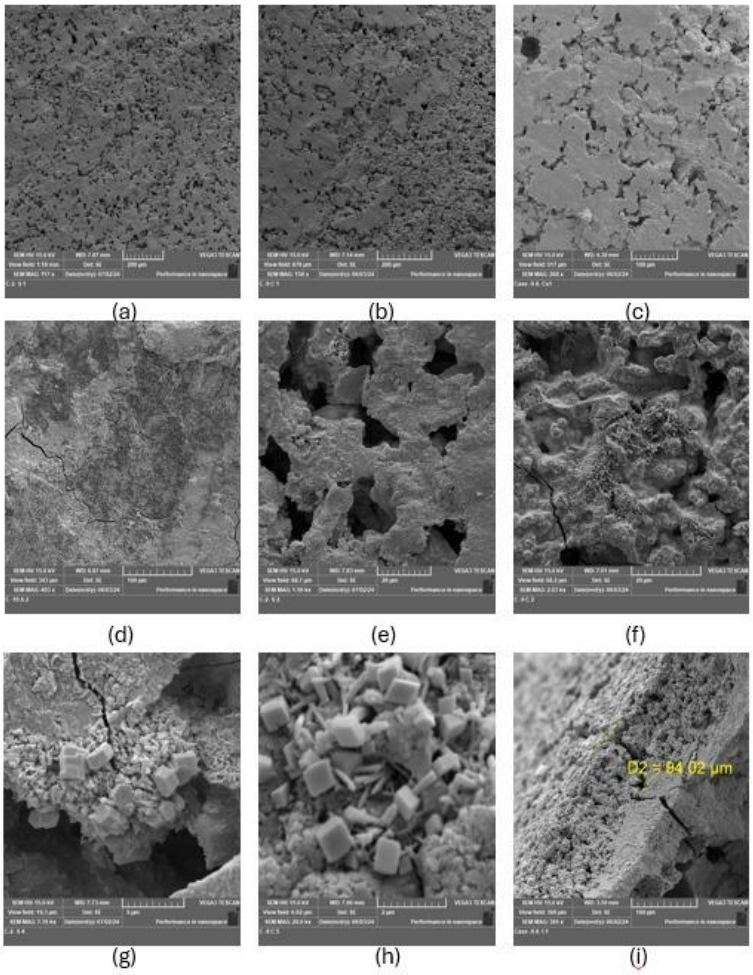

Figure 26: Microscopic investigation by SEM

5. CONCLUSIONS AND RECOMMENDATIONS

5.1 Conclusions

1. Macro-cell and Micro-cell corrosion current density
   - increases with the increase in chloride s in concrete.
   - increases with the increase in porosity of the ITZ.
   - is formed with a weaker interface as anode and denser interface as cathode.

2. Micro-cell corrosion current density increases in extreme rough condition i.e. submerged condition in sea water.

3. Concrete resistance decreases with respect to time.

5.2 Recommendations

For superior reinforced concrete durability, this thesis recommends usage of cement coating on rebar with low water cement ratio and less chloride concentration in concrete mixture but further research on combined effects, monitoring and novel mitigation strategies are required.

6. REFERENCES

1. CEMBUREAU. (2008). “Activity report 2007.” The European Cement Association, Brussels, Belgium, Activity report (Jan. 12, 2013).

2. Arya, C., Ofori-Darko, F.K., Influence of Crack Frequency on Reinforcement Corrosion in Concrete, Cement and Concrete Research, Vol. 26, No.3, 1996, pp. 345-353.
3. Mohammed, T.U., Otsuki. N., Hisada. M., and Shibata. T., Effect of crack width and bar types on corrosion of steel in concrete, ASCE Journal of Materials in Civil Engineering, 13(3), 2001, pp. 194-201.
4. Schiessl P., Raupach. M., Laboratory Studies and Calculations on the Influence of Crack Width on Chloride-Induced Corrosion of Steel in Concrete, ACI Material Journal, Vol. 94, No.1, 1997, pp. 56-61.
5. Wang. J. Wang. Q., Zhao. Y., Research progress of macrocell corrosion of steel rebar in concrete, Journal Coatings 2023, 13, 853. https:// doi.org/10.3390/coatings13050853
6. Michele, W.T.M.; Pieter, D.; Janet, M.L. Corrosion-induced cracking and bond strength in reinforced concrete. Constr. Build. Mater. 2019, 208, 228–241.
7. Song. G., and Ahmad Shayan. Corrosion of steel in concrete: causes, detection and prediction: a state-of-the-art review. No. 4. 1998.
8. Natkunarajah, K.; Masilamani, K.; Maheswaran, S.; Lothenbach, B.; Amarasinghe, D.A.S.; Attygalle, D. Analysis of the trend of pH changes of concrete pore solution during the hydration by various analytical methods. Cem. Concr. Res. 2022, 156, 106780.
9. Wang. J., Wang. Q., Zhao. Y., Zou. G. Research progress of macrocell corrosion of steel rebar in concrete. Coatings. 2023,13(5),853.
10. Grengg, C.; Müller, B.; Staudinger, C.; Mittermayr, F.; Breininger, J.; Ungerböck, B.; Borisov, S.M.; Mayr, T.; Dietzel, M. Higher solution optical pH imaging of concrete exposed to chemically corrosive environments. Cem. Concr. Res. 2019, 116, 231–237.
11. Feng, Y.; Yang, J.; Zhang, P. Effects of carbonation curing regimes on alkalinity of self-compacting concretes for marine artificial reef. Constr. Build. Mater. 2023, 369, 130614.
12. Yao, N.; Zhou, X.; Liu, Y.; Shi, J. Synergistic effect of red mud and fly ash on passivation and corrosion resistance of 304 stainless steel in alkaline concrete pore solutions. Cem. Concr. Comp. 2022, 132, 104637.
13. Torbati-Sarraf, H.; Poursaee, A. Study of the passivation of carbon steel in simulated concrete pore solution using scanning electrochemical microscope (SECM). Materialia 2018, 2, 19–22

14. Dong, Z.; Amir, P. Corrosion behavior of coupled active and passive reinforcing steels in simulated concrete pore solution. Constr. Build. Mate. 2020, 240, 117955.
15. Zheng, H.; Dai, J.; Hou, L.; Meng, G.; Poon, C.S.; Li, W. Enhanced passivation of galvanized steel bars in nano-silica modified cement mortars. Cem. Concr. Comp. 2020, 111, 103626.
16. Ghods, P.; Isgor, B.O.; Brown, J.R.; Bensebaa, F.; Kingston, D. XPS depth profiling study on the passive oxide film of carbon steel in saturated calcium hydroxide solution and the effect of chloride on the film properties. Appl. Surf. Sci. 2011, 257, 4669– 4677.
17. Ai, Z.; Jiang, J.; Sun, W.; Jiang, X.; Yu, B.; Wang, K.; Zhang, Z.; Song, D.; Ma, H.; Zhang, J. Enhanced passivation of alloy corrosion-resistant steel Cr10Mo1 under carbonation—Passive film formation, the kinetics and mechanism analysis. Cem. Concr. Comp. 2018, 92, 178–187.
18. Olsson, C.; Landolt, D. Passive films on stainless steels-chemistry, structure and growth. Electrochim. Acta 2003, 48, 1093–1104.
19. Narayanan. S., Corrosion problem of reinforced concrete and its mitigation, 2023.
20. Koch, G. H., Brongers, M. P., Thompson, N. G., Virmani, Y. P., and Payer, J. H. (2002). Corrosion Cost and Preventive Strategies in the United States, Federal Highway Administration, Washington, DC.
21. Qiao, Y.; Wang, X.; Yang, L.; Wang, X.; Chen, J.; Wang, Z.; Zhou, H.; Zou, J.; Wang, F. Effect of aging treatment on microstructure and corrosion behavior of a Fe–18Cr–15Mn–0.66N stainless steel. J. Mater. Sci. Technol. 2022, 107, 197–206.
22. B. Elsener, “Macrocell corrosion of steel in concrete-implications for corrosion monitoring,” cement & Concrete Composites, vol. 24, no. 1,pp.65-72, Feb.2002,doi:10.1016/s0958-9465(01)00027-0
23. Ghods, P.; Isgor, B.O.; Brown, J.R.; Bensebaa, F.; Kingston, D. XPS depth profiling study on the passive oxide film of carbon steel in saturated calcium hydroxide solution and the effect of chloride on the film properties. Appl. Surf. Sci. 2011, 257, 4669– 4677.
24. Ai, Z.; Jiang, J.; Sun, W.; Jiang, X.; Yu, B.; Wang, K.; Zhang, Z.; Song, D.; Ma, H.; Zhang, J. Enhanced passivation of alloy corrosion-resistant steel Cr10Mo1 under carbonation—Passive film formation, the kinetics and mechanism analysis. Cem. Concr. Comp. 2018, 92, 178–187.
25. Olsson, C.; Landolt, D. Passive films on stainless steels-chemistry, structure and growth. Electrochim. Acta 2003, 48, 1093–1104
26. C.M. Hansson, A. Poursaee, A. Laurent, Macrocell and microcell corrosion of steel in ordinary Portland cement and high-performance concretes, Cement and Concrete Research, Volume 36, Issue 11,2006, Pages 2098-2102, ISSN 0008-8846.

27. ASTM C 39/ C39M–16. Standard Test Method for Compressive Strength of Cylindrical Concrete Specimen. West Conshohocken: ASTM International, 2016.
28. Michele, W.T.M.; Pieter, D.; Janet, M.L. Corrosion-induced cracking and bond strength in reinforced concrete. Constr. Build. Mater. 2019, 208, 228–241.
29. ASTM C 39/ C39M–16. Standard Test Method for Compressive Strength of Cylindrical Concrete Specimen. West Conshohocken: ASTM International, 2016.
30. Sandra N, Kawaai K, Ujike I. Corrosion current density of macrocell of horizontal steel bars in reinforced concrete column specimen. International Journal of GEOMATE, 2019, 16(54): 123−128
31. Nanayakkara O, Kato Y. Macro-cell corrosion in reinforcement of concrete under non-homogeneous chloride environment. Journal of Advanced Concrete Technology, 2009, 7(1): 31−40
32. Mohammed T U, Otsuki N, Hamada H, Yamaji T. Macro-cell and micro-cell corrosions of steel bars in cracked concrete exposed to marine environment. In:5th CANMET/ACI International Conference on Recent Advances in Concrete Technology. Farmington Hills, MI: ACI International, 2011: 55−169
33. Inderyas. O., Tufail. M. Perfromance evaluation of high performance concrete in non-destructive and destructive testing. Ciência e Técnica Vitivinícola, 2016.
34. Alonso C, Andrade C, Gonzalez J A. Relation between resistivity and corrosion rate of reinforcements in carbonated mortar made with several cement types. Cement and Concrete Research, 1988, 18(5): 687−698
35. Alonso. C., Andrade. C., Gonzalez. J. A. Relation between resistivity and corrosion rate of reinforcemnets in carbonated mortar made with several cement types. Cement and Concrete Research, 1988, 18(5): 687-698
36. Sanchez. A., Bosch. J., Belin. R. Corrosion behavior of steel -reinforced green concrete containing recycled coarse aggregate additions in sulfate media. Materials 13(19):4345.
37. Wei Luo, Tiejun Liu, Weijie Li, Dujian Zou, Qiaoyi Chen, An electromechanical impedance-based sensor for monitoring the pitting corrosion of steel: Simulation with experimental validation, Sensors and Actuators A: Physical, Volume 376, 2024, 115585, ISSN 0924-4247.